Phytopathology® • 2023 • 113:44-54 • https://doi.org/10.1094/PHYTO-03-22-0086-R

Fungal Biology and Genetics

Hyperspectral Imaging in the UV Range Allows for Differentiation of Sugar Beet Diseases Based on Changes in Secondary Plant Metabolites

Anna Brugger,[1] Facundo Ispizua Yamati,[2] Abel Barreto,[2] Stefan Paulus,[2] Patrick Schramowsk,[3] Kristian Kersting,[3] Ulrike Steiner,[1] Susanne Neugart,[4] and Anne-Katrin Mahlein[2,†]

[1] University of Bonn, Institute for Crop Science and Resource Conservation (INRES)–Plant Pathology, Bonn, 53115, Germany
[2] Institute of Sugar Beet Research, Goettingen, 37079, Germany
[3] Technical University Darmstadt, Computer Science Department and Centre for Cognitive Science, Darmstadt, 64289, Germany
[4] University of Goettingen, Division of Quality and Sensory of Plant Products, Goettingen, 37075, Germany
Accepted for publication 28 July 2022.

Abstract

Fungal infections trigger defense or signaling responses in plants, leading to various changes in plant metabolites. The changes in metabolites, for example chlorophyll or flavonoids, have long been detectable using time-consuming destructive analytical methods including high-performance liquid chromatography or photometric determination. Recent plant phenotyping studies have revealed that hyperspectral imaging (HSI) in the UV range can be used to link spectral changes with changes in plant metabolites. To compare established destructive analytical methods with new nondestructive hyperspectral measurements, the interaction between sugar beet leaves and the pathogens *Cercospora beticola*, which causes Cercospora leaf spot disease (CLS), and *Uromyces betae*, which causes sugar beet rust (BR), was investigated. With the help of destructive analyses, we showed that both diseases have different effects on chlorophylls, carotenoids, flavonoids, and several phenols. Nondestructive hyperspectral measurements in the UV range revealed different effects of CLS and BR on plant metabolites resulting in distinct reflectance patterns. Both diseases resulted in specific spectral changes that allowed differentiation between the two diseases. Machine learning algorithms enabled the differentiation between the symptom classes and recognition of the two sugar beet diseases. Feature importance analysis identified specific wavelengths important to the classification, highlighting the utility of the UV range. The study demonstrates that HSI in the UV range is a promising, nondestructive tool to investigate the influence of plant diseases on plant physiology and biochemistry.

Keywords: high-performance liquid chromatography, hyperspectral imaging, machine learning, plant metabolites, sugar beet, UV range

Plants are exposed to various biotic stress, in particular herbivores, pests, and pathogens. In response, plants can up- or downregulate secondary plant metabolites, which play an important role in the defense against biotic stress. Secondary plant metabolites have a low molecular weight and are generally classified as nonessential for plants (Pusztahelyi et al. 2015). The secondary plant metabolite group of phenolics all derive from shikimic acid and include, among other flavonoids, catechols, and tannins (Bennett and Wallsgrove 1994).

Important groups of flavonoids are classified as preformed and induced flavonoids (Treutter 2006). Preformed flavonoids are produced during normal development of the leaves and stored at sites where they have important signaling or defense roles. For example, preformed flavonoids are stored in epidermal cells to be rapidly released into stressed tissue (Beckmann 2000). In contrast, induced flavonoids are produced as a reaction to abiotic or biotic stress and are known to play an important role in the plant's resistance to pathogens (Treutter 2006). In addition, flavonoids are produced as protection against UV light, as a color for flowers, or as signal molecules (Beckmann 2000). UV-light stress leads to an increase of the flavonoids kaempferol and pelargonidin (Monici et al. 1993). In contrast, drought stress in grapevine seedlings leads to a decrease in the phenolic acids caffeic acid and ferulic acid in the leaves (Król et al. 2014), and barley mutants resistant to *Fusarium* produce proanthocyanidins subsequent to an infection (Skadhauge et al. 1997). Pearl millet genotypes resistant to downy mildew and tomato cultivars resistant to *Verticillium alboatrum* displayed a decrease in total phenol content due to increased biosynthesis of lignin (Mahatma et al. 2011; Pollock and Drysdale 1976). Changes in flavonoids enable conclusions to be drawn regarding the health of the plant. Since flavonoids exhibit maximum absorption at 240 to 290 nm and 310 to 370 nm, changes can be determined by spectrophotometric methods (Taniguchi and Lindsey 2018). However, spectrophotometric methods only allow identification of the generic compound class, and detection and quantification of individual flavonoid compounds relies on analytical chromatographic methods, for example, high performance liquid chromatography (HPLC) (Csepregi et al. 2013). HPLC allows for the analysis of a range of phenolic acids including gallic acid, ferulic acid, caffeic acid, and flavonoids including catechin, rutin, and quercetin in plant leaves (Kowalski and Wolski 2003). In addition to flavonoids, pigments including chlorophylls and carotenoids can be used to rate plant stress, since biotic stress results in a downregulation of genes for pigment synthesis that can help the initiation of a defensive

†Corresponding author: A.-K. Mahlein; mahlein@ifz-goettingen.de

Author contributions: A.B., F.I.Y., S.P., P.S., K.K., U.S., S.N., and A.K.M. designed the study and interpreted the data. A.B. maintained the plant material, carried out the measurements and extraction. S.N. carried out HPLC-analysis. A.B. and F.I.Y. carried out the spectral data analysis. F.I.Y., A.B.A., P.S., and K.K. conducted the feature importance analysis. A.B. and F.I.Y. drafted the manuscript. U.S., K.K., and A.K.M. directed the research and gave initial input. All authors read and approved the final manuscript.

Funding: Support was provided through funds by the German Federal Ministry of Food and Agriculture (BMEL) based on a decision of the Parliament of the Federal Republic of Germany via the Federal Office for Agriculture and Food (BLE) under the innovation support program (project "DePhenSe"; grant 2818204715). This study was partially funded by the Deutsche Forschungsgemeinschaft (DFG, German Research Foundation) under Germany's Excellence Strategy (grant 2070-390732324).

The author(s) declare no conflict of interest.

reaction (Bilgin et al. 2010). Chlorophylls and carotenoids present maximum absorption from 400 to 500 nm (Taniguchi and Lindsey 2018). The various pigments can be easily extracted from leaves to determine their quantities (Scholes et al. 1994). In sugar beet (*Beta vulgaris*) several phenols have been identified, including hydroxybenzoic acid and other phenolic compounds in Swiss chard leaves (Pyo et al. 2004), and flavonoids including quercetin, which is in the subclass of flavonols (Gil et al. 1998).

Two important foliar fungal pathogens of sugar beet that cause biotic stress and changes in pigments, as well as flavonoids, are *Cercospora beticola* causing Cercospora leaf spot (CLS) and *Uromyces betae* causing sugar beet rust (BR). *C. beticola* enters the leaf through the stomata and initially colonizes the tissue asymptomatically. During pathogenesis, the toxins cercosporin and beticolin are produced that necrotize the plant cells, which eventually collapse. Melanized conidiophores are produced in the center of the lesion, followed by the production of conidia (Windels et al. 1998). Urediniospores of *U. betae* enter the leaf through stomata, causing swollen, chlorotic spots as the spores accumulate under the epidermis. The spots become brown as the spores mature and reach the epidermal layer, which ruptures, and the urediniospores are released (Kristoffersen et al. 2018). Pathogenesis of both CLS and BR is subepidermal, but *U. betae* is a biotroph that causes rupturing of the epidermis to release spores outside the leaves, while *C. beticola* is a necrotroph using toxins to degrade cells. Previous studies showed that total chlorophyll and carotenoid content of sugar beet leaves infected with *C. beticola* decreased as infection progressed (Joudi et al. 2018). In contrast, *U. betae* is dependent on living plant tissue, the suppression of plant defense responses, and the reprogramming of the plant's metabolism. Furthermore, rust fungi are known to have high carotenoid contents (Davoli and Weber 2002). Other fungi, for example *Venturia inaequalis* infecting apple, cause an increase in phenolic compounds including flavonols (Petkovšek et al. 2008). Further, rust spores feature melanin-like pigments in the uredospore wall (Trocha et al. 1974). Caffeic acid as well as ferulic acid are known to feature antifungal characteristics, for example against *Botrytis cinerea* and *Sclerotinia sclerotiorum* (Ravn et al. 1989).

Changes in secondary plant metabolites and pigments caused by fungal plant diseases lead to changes in the optical properties of leaves, which can be detected using a variety of methods. Several studies have previously used hyperspectral cameras in the visible (400 to 700 nm) and infrared (700 to 1,000 nm) range to examine changes in the spectra from sugar beet leaves infected with either *C. beticola* or *U. betae* (Leucker et al. 2017; Mahlein et al. 2010, 2013) or other pathogens including *Rhizoctonia solani* (Barreto et al. 2020). Hyperspectral microscopy has been used to quantify *C. beticola* sporulation to assess CLS resistance (Leucker et al. 2017). Mahlein et al. (2010) demonstrated that different leaf diseases of sugar beet could be distinguished using hyperspectral imaging (HSI) based on unique changes in characteristics of reflectance. For example, CLS caused an increase in reflectance between 400 and 700 nm and a decrease between 700 and 900 nm, while BR exhibited similar reflectance in diseased and healthy leaves (Mahlein et al. 2012). Differentiation between diseases is also possible using a combination of at least two vegetation indices, for example the normalized difference vegetation index and anthocyanin reflectance index (Mahlein et al. 2010). While spectral vegetation indices for the detection and differentiation of plant diseases use only a few wavelengths providing information on specific attributes such as water status or pigment (Mahlein et al. 2013), more recently machine learning approaches, and especially deep learning approaches have been used to identify and quantify plant diseases from HSI data. However, machine learning and deep learning both require large sets of annotated, standardized, and normalized data (Schramowski et al. 2020). For example, based on machine learning, potato virus Y diseased plants were readily detected (Polder et al. 2019) and charcoal rot disease was detected in soybean stems (Nagasubramanian et al. 2019).The aforementioned studies are limited to using HSI for detection, identification, classification, and quantification of plant diseases. Changes in reflectance are explained by changes in photosynthesis, chemical composition of leaves, and structural changes. With the exception of chlorophyll and potassium, reflectance changes from imaging hyperspectral data have not been linked to individual plant metabolites (Ribeiro do Prado et al. 2018). While imaging hyperspectral data includes spectral and spatial data, non-imaging sensors lack spatial information and the measured area is not displayed. Non-imaging hyperspectral data have been used to link changes in reflectance to specific metabolites (Couture et al. 2016; Vergara-Diaz et al. 2020). In durum wheat, partial least squares regression (PLSR) was used to establish the relationship between spectral measurements and 74 specific plant metabolite based on genotype, environment, and water regime, with coefficients of determination ranging from 12.4% (isoleucine) to 81.7% (malate) (Vergara-Diaz et al. 2020).

However, these studies used wavelengths ranging from 400 to 2,500 nm. An extension of hyperspectral measurements to the UV range from 250 to 400 nm, which includes maximum absorption of secondary plant metabolites (Taniguchi and Lindsey 2018), allows for a more precise analysis of metabolite changes during pathogenesis. HSI in the UV range has been previously used to study abiotic and biotic stress in barley leaves, distinguishing different resistance reactions of barley inoculated with *Blumeria graminis* f. sp. *hordei* based on the different reflectance spectra. In addition, the changes were linked to changes in secondary plant metabolites (Brugger et al. 2021). Reflectance from CLS and BR diseased sugar beet in the UV range has not been measured using HSI. Since UV radiation can be phototoxic, measurement conditions must be previously defined to prevent phototoxicity. Brugger et al. (2021) established that 2,000 Lux was the maximum illumination for sugar beet without causing tissue damage. Although the leaves did not exhibit any macroscopic or microscopic damage after a single illumination with less than 2,000 Lux, time-series measurements revealed that multiple exposures of the same specimen to the UV radiation did result in tissue damage. Thus, no time-series measurements can be performed with the same sugar beet leaves, but simulated time-series measurements may be performed with different specimens used only once (Brugger et al. 2019a). Therefore, in this study, disease development classes were defined and used to study the influence of CLS and BR on sugar beet leaves in the UV range.

The objective of this study was firstly to investigate spectral changes of different foliar leaf diseases of sugar beet in the UV range using HSI; secondly, to determine the secondary plant metabolite content of the diseased leaves using HPLC-mass spectroscopy (MS) and photometric determination; and thirdly, to relate specific wavelengths and secondary metabolite contents to one another based on deep learning algorithms.

Materials and Methods

Plant cultivation

Sugar beet plants (cultivar Isabella, KWS GmbH, Einbeck, Germany) were grown in a greenhouse environment according to Mahlein et al. (2012) in plastic pots (13 cm diameter) in a commercial substrate (Topfsubstrat 1.5, Balster Erdenwerk GmbH, Sinntal-Altengronau, Germany), watered as necessary and fertilized weekly with 100 ml of a 0.2% solution of Poly Crescal (Aglukon GmbH, Düsseldorf, Germany).

Pathogen inoculation

Sugar beet plants were inoculated at growth stage 14 (Meier et al. 1993). Inoculum was prepared from dried leaves with symptoms of CLS from plants in the field. Leaves were wetted and incubated at 100% relative humidity (RH) for 24 h at room temperature to obtain adequate spore production. A spore suspension with 30,000 spores per ml of *C. beticola* was prepared from the sporulating

leaves. The spore suspension was sprayed on healthy leaves of the sugar beet plants using a plastic hand-held sprayer. The plants were immediately placed in plastic containers (to ensure 100% RH) in an incubator for 48 h at 25/20°C (day/night) and a photoperiod of 16 h. The plants were transferred to the greenhouse at 23/20°C (day/night) and 60 ± 10% RH. Urediniospores of *U. betae* obtained from infected sugar beet plants were collected and stored at 4°C as previously described (Mahlein et al. 2010). A spore suspension (30,0000 spores per ml) was prepared and sprayed on the leaves of the healthy plants using a plastic hand-held sprayer. The plants were again placed in plastic boxes in an incubator for 48 h at 20/18°C (day/night) and a photoperiod of 16 h before being transferred to the greenhouse at 23/20°C (day/night) and 60 ± 10% RH.

Classification of phenotypic disease development into symptom classes

The development of both CLS and BR was classified into four symptom classes: noninoculated (healthy), young, mid-age, and mature symptoms. The young symptom class of CLS was characterized by gray, sunken spots that indicated an accumulation of mycelium and occurred 7 to 10 days after inoculation (dai). The mid-age symptom class was characterized by necrotic spots (12 to 16 dai) and the mature symptom class by development of a reddish-brown margin and black dots in the lesion center that represented melanized conidiophores, which started at 17 dai (Fig. 1A). The young symptom class of BR was characterized by tiny chlorotic spots where the leaf tissue was swollen due to initial spore accumulation under the epidermis which occurred 10 to 12 dai. The mid-age symptom class of BR exhibited brown spots as the spores matured under the epidermal layer (13 to 18 dai), which later ruptured resulting in the mature symptom class (19 to 25 dai) (Fig. 1B).

Extraction of chlorophyll, carotenoids, and flavonoids

To extract chlorophyll, carotenoids, and flavonoids, inoculated and noninoculated (healthy) sugar beet leaves were collected at different times points after inoculation that related to the symptom development stages. The samples were kept in the freezer (−80°C) until analysis.

For chlorophyll and carotenoid extraction, approximately 1 g of frozen leaves was ground with 0.5 M perchloric acid (Merck, Darmstadt, Germany) in liquid nitrogen. Extraction was performed according to Scholes et al. (1994). A 0.5-g ground sample was mixed with 1.5 ml of 80% acetone in a tube, stored on ice for 3 h in the dark, and agitated every 20 min. The samples were centrifuged at 13,000 rpm for 20 min at 4°C, when the absorption of the extract was measured at 470, 645, and 663 nm against a blank solution of acetone. The chlorophyll and carotenoid concentrations were calculated according to Hiscox and Israelstam (1979). There were 12 replicate samples tested for each symptom class. Each sample consisted of three sugar beet leaves from an individual plant.

The total flavonoid content was extracted according to Mihai et al. (2010), and frozen leaves were ground in liquid nitrogen. A 1-g ground sample was mixed with 30 ml of 96% ethanol and held overnight with constant stirring. The extract was filtered three times using plain disc qualitative filter paper with a diameter of 8.5 cm and a retention volume of 4 to 7 µm. The volume was adjusted to 100 ml with 96% ethanol for an initial extract concentration of 1%. A 3-ml aliquot of the extract was mixed with 1 ml of 2.5% $ZrOCl_2$ (Merck), to which 21 ml of methanol was added. After 30 min, the absorption was measured at 288 nm against a blank solution of methanol. To calculate the quantity of extracted flavonoids, a calibration curve was established using chrysin (Merck). A stock solution with 0.1 mg/ml chrysin in methanol was prepared and aliquots of 0.25, 0.5, 1, 1.5, and 2 ml were each made up to 10 ml with methanol and used to develop the calibration curve. There were 12 replicate samples tested for each symptom class. Each sample consisted of one sugar beet leaf from an individual plant.

The statistical analysis of the data was performed with SigmaPlot 13.0 (Systat Software Inc., Chicago, U.S.A.) with the four symptom classes of CLS and BR serving as independent variables and chlorophyll, carotenoid, and flavonoid content as dependent variables. The normal distribution of the data was tested with the nonparametric Kolmogorov-Smirnov test, using a distribution $P \leq 0.05$. After ensuring the data were normally distributed, a one-way analysis of variance was performed with a post hoc Tukey's honestly significant difference test to determine whether differences between means were significantly different ($\alpha = 0.05$).

Extraction and identification of phenols by HPLC-MS

Phenolic compounds were extracted according to Schmidt et al. (2010) with the modifications described by Santin et al. (2018). Inoculated and noninoculated sugar beet leaves were collected at the different symptom stages and immediately placed in the freezer (−20°C) until further processing. Each frozen sample was first lyophilized and then ground as described above. A 0.02-g ground sample was mixed with 600 µl of 60% aqueous methanol and shaken at 1,400 rpm for 40 min at 20°C before the extract was centrifuged for 10 min at 4,500 rpm. The supernatant was removed, collected in a reaction tube, and stored at 4°C. The pellet was used to repeat the extraction step twice, using 300 µl of 60% aqueous methanol with the sample being shaken at 1,400 rpm for 15 min, respectively. The supernatant was collected in the same reaction tube after each extraction step and evaporated in a vacuum centrifuge. The dried residue was dissolved in 200 µl of 10% aqueous methanol before transfer to a Corning Costar Spin-X plastic centrifuge tube filter (Sigma Aldrich Chemical Co., St. Louis, MO, U.S.A.) and centrifuged at 3,000 rpm for 5 min at 20°C. The HPLC-MS measurements were performed according to Santin et al. (2018). For each symptom class, there were three replicate samples. Each sample consisted of one sugar beet leaf from an individual plant.

Hyperspectral image acquisition in the UV range

Following the approach of Brugger et al. (2019b), spectral reflectance in the UV range was recorded with a Hyperspec UV-VIS CCD Sensor (Headwall Photonics, Bolton, MA, U.S.A.) in

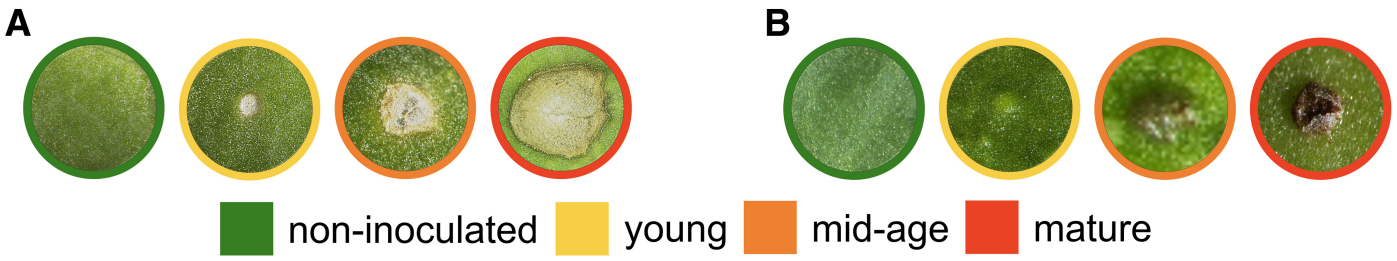

Fig. 1. Red green blue images of disease symptom progress of **A,** Cercospora leaf spot (CLS) and **B,** brown rust (BR) divided into four symptom age classes on leaves of sugar beet. Leaves were either noninoculated (healthy) or showed young, mid-age, or mature symptoms of the two diseases.

the 250 to 500 nm range. Illumination was provided by a UV lamp (UniLux, Guardian, Saddle Brook, NJ, USA) with a 21 DC halogen lamp (TechniQuip, Pleasanton, CA, U.S.A.). Image capture had an exposure time of 800 ms, a frame rate of 0.4 frames per second, and a linear axis speed of 0.2 mm/s. Using the software Headwall Hyperspec III (Headwall Photonics, Bolton, MA, U.S.A.), the relative reflectance was calculated against a white reference image of 95% barium sulfate and a dark current image (Paulus and Mahlein 2020). ENVI 5.5 (Exelis Visual Information Solutions, Boulder, CO, U.S.A.) was used to analyze the data and an 800 pixel area was used to calculate the average reflectance of each wavelength. Data were preprocessed with a Savitzky-Golay filter with a window size of 7 and a third degree polynomial. SigmaPlot 14 (Systat Software GmbH, Erkrath, Germany) was used to prepare the figures. Between 50 and 200 images were collected for each symptom class.

Machine learning

Machine learning was performed in R (R Core Team 2020) using the package *Caret* (Kuhn 2020). The feature importance using the VarImp function of the *Caret* package was conducted according to Kuhn (2012). The reflection average of approximately 800 pixels from each of the 1,330 images was used. Before processing, the data were centered and scaled where centering was the mean of the predictor's data subtracted from the predictor's value, and scaling was the value divided by the standard deviation. During the preprocessing, the data were separated according to disease and symptom class. All missing, noisy, and inconsistent data were removed.

Disease classification. The data consisted of 400 images of CLS and 837 images of BR and was split into two subsets. The first, with 80% of the data, was to train the multiclass model, and the second, with 20% of the data, was used to validate the model. Class imbalance was resolved by up-sampling in which the minority class was randomly sampled to be the same size as the majority class. Once preprocessed, random forest (rF) algorithms were used for classification. A grid search was used for hyperparameter optimization. A repeated K-fold cross validation was implemented to improve the estimated performance of the model, with five repeats of 10-fold. K-fold validation was performed on the training dataset and the best model hyperparameters were identified.

Clustering. Once the models were obtained, the respective importance of each variable was extracted. For permutation, the approach used followed that described in the R package *random Forest* (Liaw and Wiener 2002). The prediction accuracy for each tree was recorded and averaged over all trees after permuting each predictor variable. To determine the degree of spectral similarity for the different symptom classes for CLS and BR, data were normalized, and the pairwise Earth mover's distance (EMD) score was determined for all possible combinations of the classes using EMDomics (Nabavi et al. 2016). Once the EMD score was obtained, a hierarchical clustering was determined. To display this, a dendrogram was prepared in R using the package *Dendextend* (Galili 2015). The dendrogram highlights the similarities between the different diseases and symptom classes, allowing visualization and comparison of the trees determined by the hierarchical clustering. All spectral data in the entire wavelength range were used to create the dendrogram.

Metabolites classification and regression. To predict metabolites in sugar beet leaves from the HSI data, three regression models were used including the rF, K-nearest neighbors (KNN), and partial least square (PLS). HSI data and analytical results used for the regression were generated from two different sets of samples since UV radiation causes tissue damage on sugar beet leaves (as noted previously). To exclude changes in metabolites caused by the UV radiation, strict symptom classes were defined, and samples were chosen accordingly for both sets. For data preprocessing, centering and scaling settings were used. No upsampling or downsampling was used. Each model was trained for each disease and each metabolite. The final model accuracy in Table 1 is an average of the number of repetitions. A repeated K-fold cross validation was implemented to improve the estimated performance of the model, with 10 repeats of threefold.

Results

Secondary metabolite profiles revealed changes depending on pathogen

The highest values of chlorophyll, carotenoid, and flavonoid content were measured in noninoculated leaf samples (Fig. 2). While noninoculated leaves had a total chlorophyll content of 7.5 µg/ml, leaves with young CLS symptoms had a lower chlorophyll content of 4.7 µg/ml, which decreased progressively with leaves with mature symptoms having a chlorophyll content of 4.1 µg/ml. Leaves with young BR symptoms exhibited the lowest chlorophyll content of 2.7 µg/ml, which increased to 4.8 µg/ml in leaves with mature symptoms. A similar pattern was detected for carotenoid and total flavonoid content. Leaves with young CLS symptoms had a carotenoid content of 1.5 µg/ml, which decreased to 0.9 µg/ml in leaves with mature symptoms. Leaves with young BR symptoms had a low carotenoid content of 0.7 µg/ml, but leaves with mid-age and mature symptoms had a content of 1.2 µg/ml. Leaves with young CLS symptoms had 52% total flavonoid content (mg of quercetin equivalent/g of dry weight), which decreased to 43.8% in leaves with mature symptoms, while leaves with young symptoms of BR exhibited a low flavonoid content of 51.3%, which increased to 53.6% in leaves with mature symptoms. Several phenolic acids were identified and quantified by HPLC-MS, including two caffeic acid derivatives, two ferulic acid derivatives, and two vitexin derivatives (Fig. 3). Noninoculated samples of leaves had a total phenolic acids content of 36 mg/g dry weight, which declined to 5.5 mg/g dry weight samples of leaves with young symptoms of CLS and increased again to 30 mg/g dry weight in leaves with mature symptoms. The flavonoid isorhamnetin-dihexoside presented a similar value in leaf samples of all symptom classes except in leaf samples with young symptoms. All other phenolic acids showed a change in content depending on the symptom age on the leaf sample. Samples of leaves with young symptoms of BR presented had a low total phenolic acid content of 14.5 mg/g dry weight, which increased to 49 mg/g for leaves with mid-age symptoms. The highest contents of phenolics were detected in leaves with mid-age symptoms of BR, and the phenolic with the highest content was isorhamnetin-dihexoside.

TABLE 1. Results of three different regression models used to predict chlorophyll, carotenoids, and flavonoids content from hyperspectral reflectance data[a]

Disease	Method	Metabolite	R^2	RMSE	RMSESD
Cercospora leaf spot	rF	Chlorophyll	0.89	0.44	0.15
	KNN	Chlorophyll	0.88	0.47	0.15
	PLS	Chlorophyll	0.55	0.96	0.09
	rF	Carotenoids	0.40	0.21	0.03
	KNN	Carotenoids	0.34	0.22	0.04
	PLS	Carotenoids	0.32	0.22	0.03
	rF	Flavonoids	0.73	2.47	0.39
	KNN	Flavonoids	0.67	2.77	0.49
	PLS	Flavonoids	0.5	3.43	0.47
Brown rust	rF	Chlorophyll	0.80	0.56	0.09
	KNN	Chlorophyll	0.73	0.69	0.09
	PLS	Chlorophyll	0.29	1.05	0.06
	rF	Carotenoids	0.61	0.15	0.01
	KNN	Carotenoids	0.59	0.16	0.01
	PLS	Carotenoids	0.23	0.21	0.01
	rF	Flavonoids	0.78	2.42	0.20
	KNN	Flavonoids	0.72	2.82	0.38
	PLS	Flavonoids	0.35	4.12	0.24

[a] The coefficient of determination (R^2), root-mean-square error (RMSE), and root-mean-square-error standard deviation (RMSESD) are presented. rF, random forest; KNN, K-nearest neighbors; and PLS, partial least square.

Different sugar beet diseases have different spectral patterns

The reflectance from sugar beet leaves was characterized by distinct peaks between 250 and 312 nm as well as 410 and 440 nm (Fig. 4). The highest reflectance of each sample was measured at a wavelength of 253 nm, beyond which the reflectance decreased to 420 nm. Noninoculated leaves of sugar beet had 0.4% reflectance at 253 nm and 0.09% reflectance at 500 nm. Young symptoms of CLS (Fig. 4A) had 0.5% reflectance at 253 nm, which decreased to 0.2% reflectance at 400 nm, with reflectance remaining constant to 500 nm. Similar reflectance values were observed for mature symptoms of CLS up to 400 nm, above which the reflectance increased to 0.24% at 500 nm, the highest value recorded. Mid-age symptoms had a reflectance of 0.6% at 253 nm, which decreased to 0.21% at 400 nm. From 400 to 460 nm, the reflectance was constant, but increased slightly to 0.235% at 500 nm. Leaves with young symptoms of BR had 0.48% reflectance at 253 nm, which decreased to 0.16% at 420 nm, remaining almost constant to 500 nm (Fig. 4B). Leaves with mid-age symptoms of BR had reflectance values of 0.46% at 253 nm, which decreased sharply at 350 nm, at which point reflectance values were similar to the noninoculated leaf samples. Compared to the noninoculated leaf samples, leaf samples with mid-age symptoms had slightly higher reflectance values between 480 to 500 nm. Leaves with mature symptoms of BR had similar reflectance to noninoculated leaf samples from 250 to 300 nm, but reflectance decreased more rapidly to 445 nm. Between 445 and 500 nm, reflectance was approximately 0.11%, similar to leaves with mid-age symptoms.

Classification of symptoms and feature importance for identifying discriminating wavelength ranges

Of all the CLS images, 1.27% of leaves with mid-age symptoms were falsely classified as young symptoms. With BR, leaves with mid-age samples were falsely classified as young symptoms (1.06%) or noninoculated leaf samples (0.53%), and 0.53% of leaves with young symptoms were falsely classified as mid-age symptoms (Fig. 5). To demonstrate the similarity among the classes, a dendrogram was created based on the mean spectra (Fig. 6). The dendrogram exhibits two main clusters. A high similarity was found for all BR symptom classes and the noninoculated samples. The second cluster consisted of all the CLS symptom classes. The subsequent feature importance analysis identified wavelengths that were most useful to identify the different symptom classes (Fig. 7). For the noninoculated leaves in the CLS group, wavelengths between 250 and 350 nm had a high value (100%), while leaves with young symptoms of CLS were characterized by wavelengths of 400 nm or more. In contrast, leaves with mid-age symptoms of CLS were associated with values of 60% at wavelengths from 250 to 300 nm, but only 10% at wavelengths of 420 to 430 nm. Similar to leaves with young symptoms, leaves with mature CLS symptoms were characterized by high values at wavelengths of 450 nm or more. For noninoculated leaves in the BR group, the importance of the wavelength decreased from 250 nm (80%) to 11% at 500 nm. Leaves with young and mid-age symptoms of BR had high values with wavelengths from 320 to 410 nm (almost 100%). Leaves with mature symptoms of BR had values of 60% between 250 and 400 nm, above which the importance of the wavelengths decreased to 0% at 480 nm.

The prediction accuracy of the metabolites based on the HSI data using the different regression models ranged from weak to strong based on the coefficient of determination ($R^2 = 0.23$ to 0.89). The rF regression achieved the highest accuracy, while the least accurate method was the PLSR. Root-mean-square error values ranged from 0.21 to 4.12. For both diseases, the least accurate prediction was that for the carotenoids (Table 1).

Discussion

In the present study, HSI in the UV range was used to assess reflected spectral changes from sugar beet leaves with symptoms of CLS and BR. Both CLS and BR develop subepidermal leaf structure and influence the host plant despite differing lifestyle of the two pathogens causing the disease. Both diseases progressed as previously described (Mahlein et al. 2012) and were divided into four symptom classes since previous studies (Brugger et al. 2019a) revealed that sugar beet leaves exhibit tissue damage after HSI measurements with UV light. The precise definition of the symptom classes based on visual characteristics of the disease as it progressed allowed for appropriate hyperspectral measurements at the same times to ascertain changes in infection. Both diseases had unique changes in spectral signatures with each symptom class. While all CLS symptom classes were generally characterized by changes in reflectance at wavelengths from 250 to 410 nm and 430

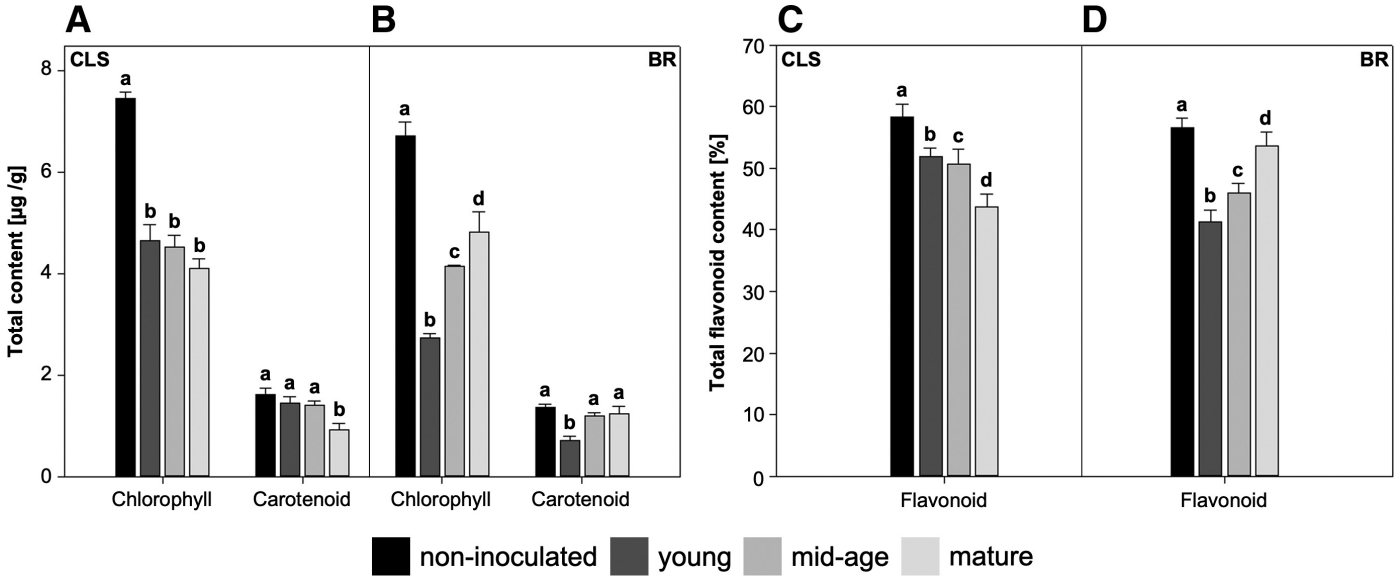

Fig. 2. Pigment and flavonoid content of leaves diseased with **A and C,** Cercospora leaf spot (CLS) and **B and D,** brown rust (BR) and classified into noninoculated leaves, and leaves with young, mid-age, or mature symptoms. Standard deviations of the means are indicated. For each secondary metabolite, means with different lowercase letters are significantly different according to Tukey's honest significant difference test ($\alpha = 0.05$). Means are based on 12 samples for each symptom class.

to 500 nm, BR had less pronounced changes in reflectance between the symptom classes. Different pathogens cause specific physiological changes in a plant, so differentiation between diseases is possible based on the resulting unique reflectance patterns (Jones and Dangl 2006). Perthotrophic fungi like *C. beticola* penetrate leaves through the stoma and produce toxins and hydrolytic enzymes, which leads to cell death and consequent nutrient uptake by the fungus (Knogge 1996). As a consequence, necrotic tissue develops. In contrast, rust fungi, in this case *U. betae*, are biotrophic and depend on living host tissue throughout the life cycle of the pathogen (Mahlein et al. 2010). The different strategies of the pathogens results in unique changes in spectral signatures during pathogenesis. In a previous study, CLS was characterized by an increase in reflection at wavelengths from 400 to 500 nm, while BR was characterized by constant reflection in the same range (Mahlein et al. 2012). The same patterns were observed in our study (Fig. 4), demonstrating the reliability of the hyperspectral sensor in the UV range.

There was a pronounced increase in reflectance for leaves with mid-age symptoms of CLS at wavelengths from 250 to 350 nm, which can be linked to a decrease in flavonoids. In the early stages of infection, the plant attempts to defend itself against the pathogen, which can lead to changes similar to those seen in a resistance response, as characterized in previous studies by an increase in total phenolic content due to increased lignin synthesis (Mahatma et al. 2011; Pollock and Drysdale 1976). As the infection progresses, the synthesis of lignin declines, resulting in a higher phenols content, which is characterized by lower reflectance values with leaves having mature CLS symptoms. The increase in reflection we observed with CLS at wavelengths of 430 to 500 nm can be associated with the decrease in total chlorophyll content, and the decrease in carotenoid content (Joudi et al. 2018).

In contrast, BR results in only small changes in reflectance, with the highest reflectance values measured from leaves with young symptoms. An increase in reflectance for leaves with young symptoms at wavelengths from 250 to 400 nm can be associated with decreasing flavonoid content, which are known to decrease due to infection with rust fungi (Lu et al. 2017). In addition, previous studies revealed that rust fungi cause higher level of carotenoids in host tissue (Davoli and Weber 2002), which would be associated with a decrease in reflectance in the visible range. In the current study, only the leaves with young symptoms had a slightly increased reflectance in the range of 430 to 500 nm, and at this early stage of infection, no change in carotenoid levels has been observed in other studies. The similar reflectance values of BR symptom classes in the range from 400 to 500 nm can be attributed to the small size of rust symptoms (approximately 1 mm in diameter). In addition, low resolution HSI cameras can lead to a mixed reflectance from healthy tissue and rust symptoms, making the evaluation of the measurements more challenging. The biotrophic fungus *U. betae* is dependent on living plant cells for nutrition uptake, so structural changes to the host are likely minimal during early infection, and consequently only minor changes occur with pigment contents (Mahlein et al. 2012).

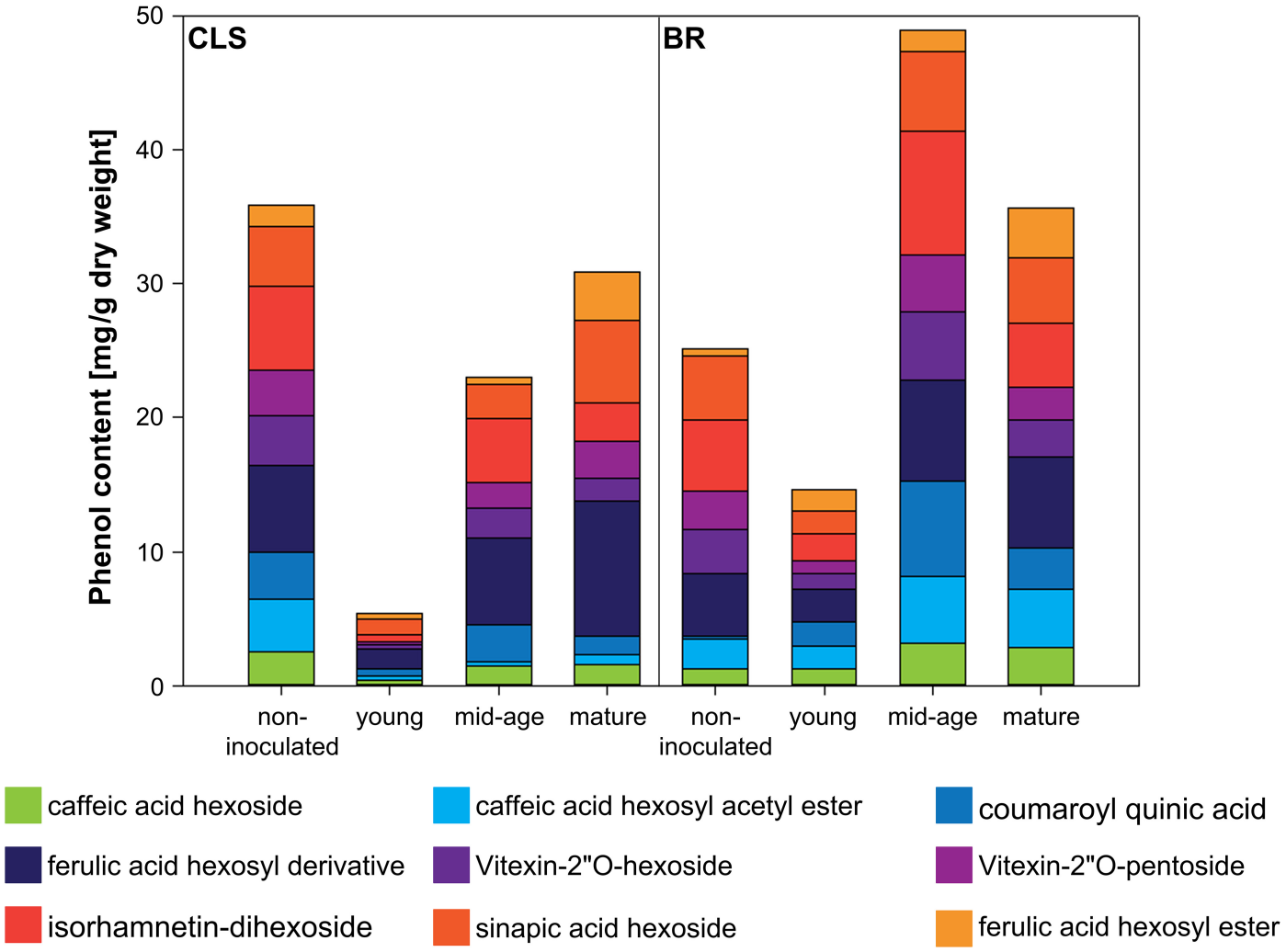

Fig. 3. Phenolic acid content of leaves diseased with Cercospora leaf spot (CLS) or brown rust (BR) and classified into noninoculated leaves, and leaves with young, mid-age, or mature symptoms.

Spectral changes recorded with hyperspectral measurements depending on the fungal pathogen and time course of infection were associated with metabolite contents to study the extent to which spectral changes reflect changes in plant metabolites. It is known that leaf metabolites, including chlorophyll and carotenoids, decrease if plants are infected by pathogens that cause necrotic symptoms, such as CLS (Jing et al. 2007; Joudi et al. 2018). We similarly observed that the highest total chlorophyll and carotenoid contents were measured in healthy leaves, and the metabolites decreased during disease development. It is notable that leaves with young and mid-age CLS symptoms had only minor differences in spectral reflectance and metabolite content. The substantial decrease in metabolites in leaves with young symptoms of BR can be explained by the chlorosis resulting from the development of spores under the epidermis. In contrast, the increase in chlorophyll and carotenoids of leaves with mid-age and mature symptoms of BR might result

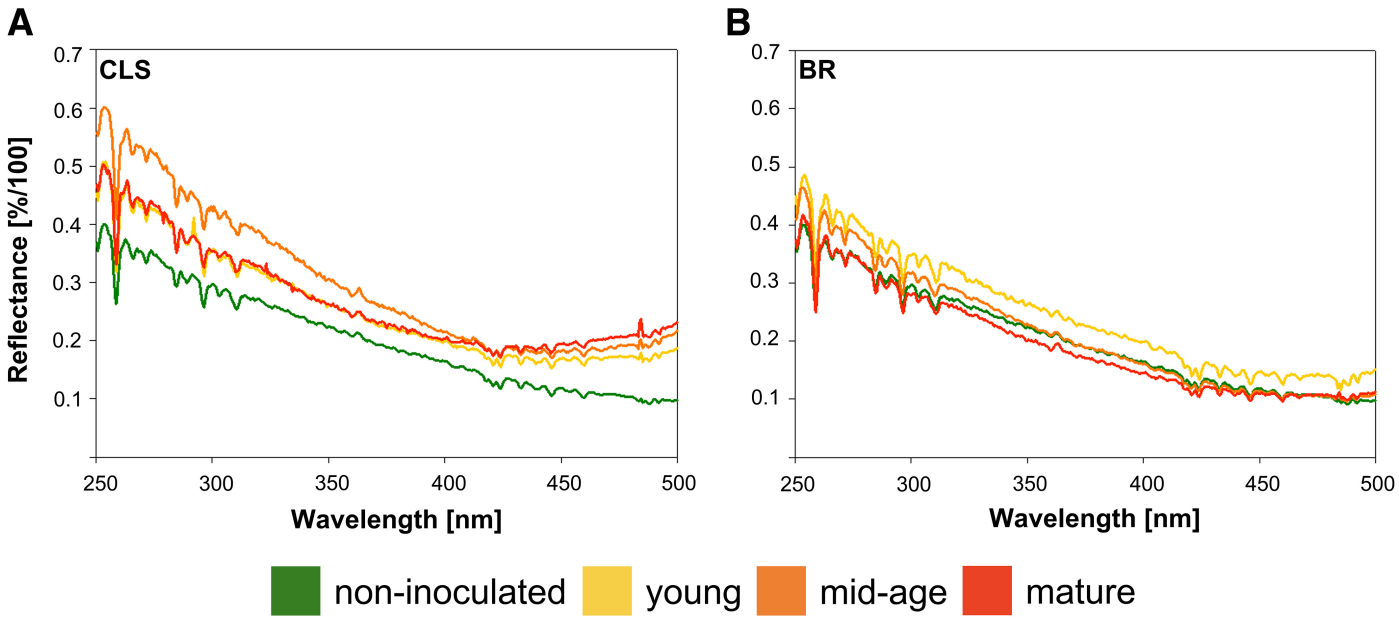

Fig. 4. Hyperspectral signatures over the UV range for leaves of sugar beet for each symptom age class of the two diseases **A,** Cercospora leaf spot (CLS) and **B,** brown rust (BR). All spectral signatures were characterized by a high reflectance value at 250 nm and a decrease in reflectance to 450 nm (CLS) or 500 nm (BR).

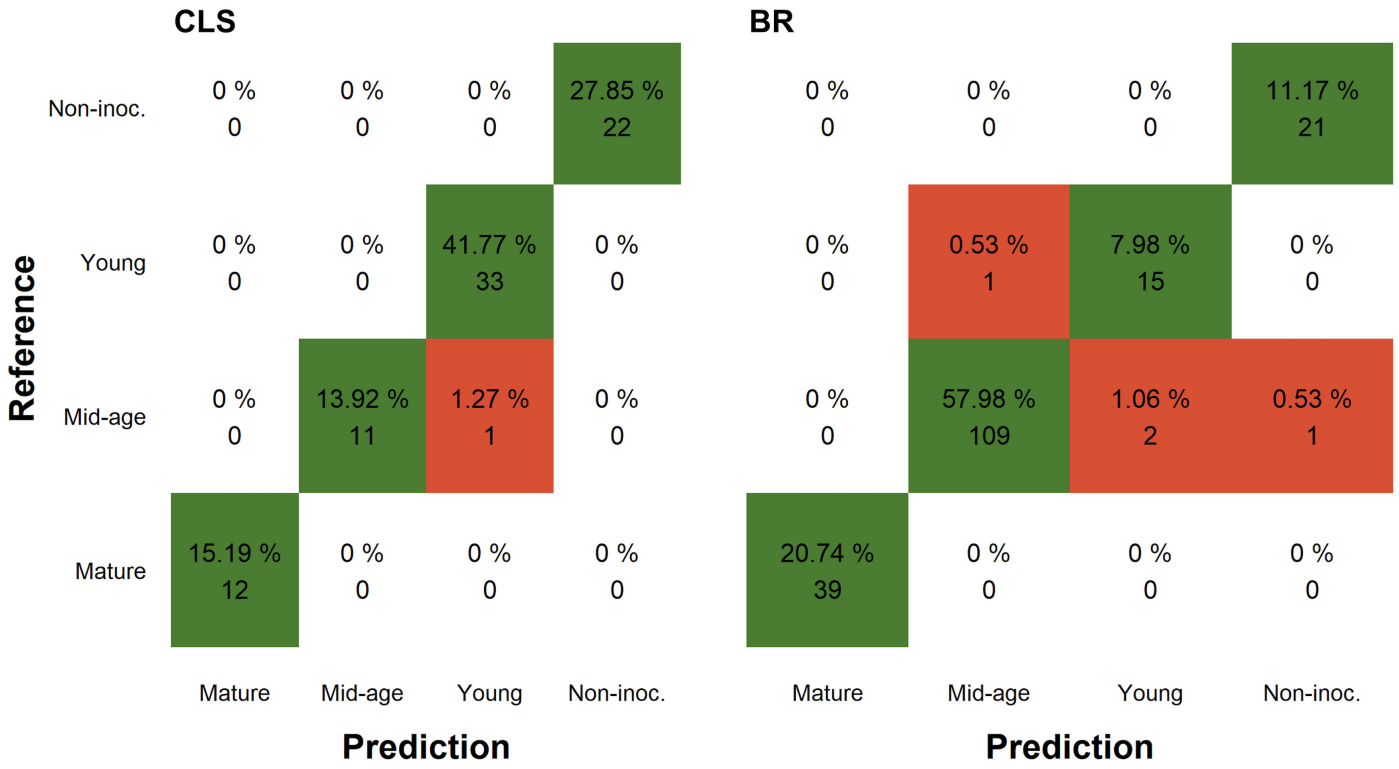

Fig. 5. A confusion matrix showing the results of the random forest classification based on hyperspectral imaging data to classify different disease symptom classes of Cercospora leaf spot (CLS) and brown rust (BR). Green (dark gray) indicates correct classification and red (light gray) indicates incorrect classification. For CLS, leaves with mid-age symptoms were falsely classified as young symptoms, while with BR, leaves with mid-age symptoms were falsely classified as noninoculated leaves or as leaves with young symptoms, and leaves with young symptoms were falsely classified as leaves with mid-age symptoms.

from the dispersion of urediniospores (Yahya et al. 2020). The decrease in phenolic compound content, to which the flavonoids belong, has been reported as due to a high increase in lignin biosynthesis due to a resistance response (Mahatma et al. 2011; Pollock and Drysdale 1976). Although susceptible cultivars of sugar beet were used in the current study, the decrease in flavonoids in leaves with young BR symptoms may be related to a resistance reaction of the plant at the beginning of infection. However, as the symptoms progress BR leads to an increase in flavonoid content in leaves with young to mature symptoms, as described previously with other pathogens that cause an increase in flavonoids, and especially flavonols (Treutter 2006). An increase in phenolics (especially the flavonols quercetin-3-galactoside, quercetin-3-glucoside, kaempferol-3-galactoside, and isorhamnetin-3-glucoside which increased by 95%) was similarly reported for 3 days after infection of peaches with *M. fructicola* (Santin et al. 2018). HPLC analysis in the current study identified the flavonoid isorhamnetin-dihexoside, previously described in germinating rape seedlings (Jiang et al. 2013). Like other phenols, isorhamnetin-dihexoside content showed a sharp decline at the onset of infection, followed by an increase in leaves with mid-age symptoms. Secondary plant metabolites, for instance, quercetin, but also vitexin, sinapic acid, and ferulic acid, were classified as antioxidants in multiple studies and are substances that protect cells from damage by inhibiting oxidation (Natella et al. 1999). The increase in antioxidants content has been reported after the onset of necrosis in, for example, tobacco leaves inoculated with tobacco mosaic virus (Fodor et al. 1997), affirming our observations of the increase in antioxidants in sugar beet leaves with mid-age and mature symptoms of CLS and BR. Two other phenols detected by HPLC were identified as caffeic acid and coumaroyl quinic acid. Caffeic acid is methylated to ferulic acid, which is important for the synthesis of lignin (Whetten and Sederoff 1995). As mentioned above, lignin plays an essential role in resistance reactions to strengthen cell walls (Mahatma et al. 2011; Pollock and Drysdale 1976), explaining the initial decrease in content in leaves with young symptoms. Coumaroyl quinic acid is important for the synthesis of chlorogenic acid, which is essential for age-mediated changes in plant leaves (Morales et al. 2005). Since plant samples of the same age were used in our study, changes in coumaroyl quinic acid due to the aging processes can be excluded.

By using rF to determine the spectral data characteristics associated with specific symptom classes, accurate classification was achieved. False classification of leaves with mid-age symptoms of BR as noninoculated or young symptoms can be explained by the similar spectra of the two symptom classes, as presented in the dendrogram (Fig. 6). The similarity between BR symptom classes and the noninoculated leaf samples can be related to the lifestyle of the biotrophic fungus *U. betae*, which is dependent on living sugar beet leaf tissue for its survival, and therefore causes minimal damage to the host plant during the early stages of infection. The necrotrophic fungus, *C. beticola*, in contrast rapidly kills the host cells, leading to an individual cluster of the symptom classes in the dendrogram. The classification accuracy enabled differentiated feature importance, identifying important wavelengths for the classification of the two diseases and the different symptom classes. With the exception of leaves with mature symptoms of CLS, it is particularly interesting to note that the UV range from 250 to 410 nm is of high importance for differentiating the symptom classes, and we can conclude that changes in secondary plant metabolite content are more important than changes in chlorophyll and carotenoids content for differentiation of the plant−pathogen interactions. The extraction and analysis of the metabolites accentuate the various roles secondary plant metabolites play during a susceptible plant−pathogen interaction, and that they can be linked to spectral changes during symptom development. Predictive accuracy of HSI data for plant metabolites was determined to further examine the significance of reflectance values to track changes in metabolite content. Using data from field spectroradiometers and airborne imaging spectroscopy, previous studies using PLSR achieved prediction accuracies of 0.28 to 0.82 in ecoregions with temperate and subtropical forests as well as grasslands (Wang et al. 2020) and 0.124 to 0.817 for durum wheat characteristics (Vergara-Diaz et al. 2020). We achieved a high accuracy with the rF regression associated with chlorophyll ($R^2 < 0.8$) and flavonoid ($R^2 < 0.73$) content for both CLS and BR. Carotenoids in sugar beet leaves with CLS were not predicted with acceptable accuracy ($R^2 < 0.4$). Reasons for inaccuracy may be the overlapping or masking of signals of different plant metabolites with close absorption maxima or changes in metabolites that are too small to be detected reliably due to the low resolution of the camera. The relatively high predictive values ($R^2 > 0.7$) for chlorophyll and flavonoids enable correct conclusions regarding changes in some metabolites based on spectral signatures. However, in order to reliably use HS measurements in place of destructive methods for the analysis of plant metabolites,

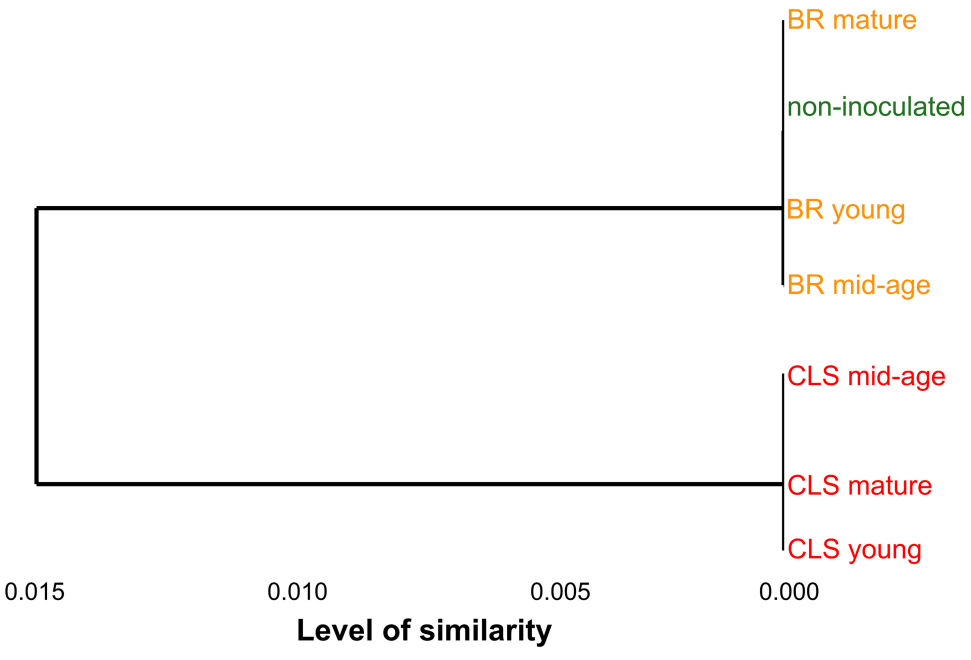

Fig. 6. Dendrogram of the spectral information showing the similarities between the different diseases and symptom classes. The similarity is represented on the x-axis and the clusters are displayed on the y-axis. There are two clusters with a high similarity. The first is between the noninoculated leaf group and all the classes of brown rust (BR) symptoms, and the second cluster includes all the classes of symptoms of Cercospora leaf spot (CLS).

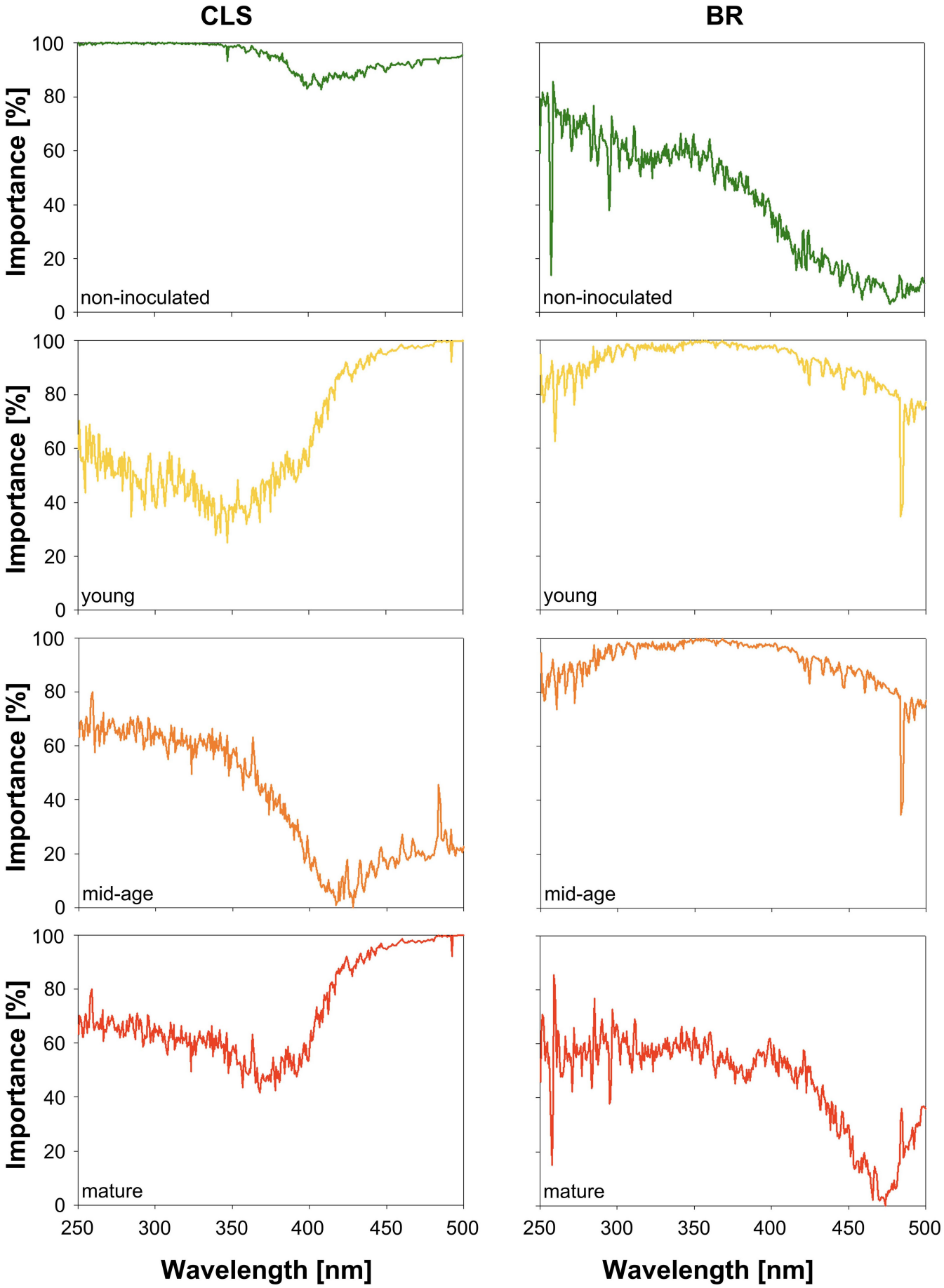

Fig. 7. Feature importance for identifying different classes of disease symptoms of Cercospora leaf spot (CLS) and brown rust (BR). The different symptom classes for CLS and BR are noninoculated leaves, and leaves with young, mid-age, or mature symptoms.

higher accuracy values ($R^2 > 0.95$) must be achieved. Nevertheless, the results of this study support the claim that HSI data in the UV range can be associated with changes in plant metabolites. While almost all spectral changes in disease progress of CLS can be confirmed by analytical studies, there were discrepancies between BR symptom development, spectral changes, and the analytical results. Reasons may include the previously mentioned size of BR symptoms, which combined with the low resolution of HSI cameras lead to challenging spectral evaluation of the symptoms due to mixed signals. However, considering destructive methods such as HPLC are costly and time-consuming, HSI in the UV range may offer an advantage for analyzing plant−pathogen interactions in some situations, for example, for breeding purposes.

The results demonstrate the potential of HSI in the UV range for identifying changes in secondary plant metabolites resulting from foliar diseases. While small symptoms associated with diseases such as BR may lead to contradictory results, spectral changes in CLS symptoms can be linked to changes in secondary metabolites. Improvements in the resolution of hyperspectral and multispectral cameras may allow accurate recognition of spectral changes for diseases that have symptoms characterized by small lesions. However, hyperspectral measurements in the UV range can already be used to differentiate between plant−pathogen interactions and our results further demonstrate the method can be used to elucidate the changes of secondary plant metabolites.

Acknowledgments

We thank Jan Behmann, Marcus Jansen, and Hans-Georg Luigs for technical support and Sabine von Tiedemann for proofreading and helpful comments on the manuscript.

Literature Cited

Barreto, A., Paulus S., Varrelmann, M., and Mahlein, A.-K. 2020. Hyperspectral imaging of symptoms induced by *Rhizoctonia solani* in sugar beet: Comparison of input data and different machine learning algorithms. J. Plant Dis. Prot. 127:441-451.

Beckmann, C. 2000.Phenolic-storing cells: Keys to programmed cell death and periderm formation in wilt disease resistance and in general defense responses in plants. Physiol. Mol. Plant Pathol. 57:101-110.

Bennett, R. N., and Wallsgrove, R. M. 1994. Secondary metabolites in plant defence mechanisms. New Phytol. 127:617-633.

Bilgin, D. D., Zavala, J. A., Zhu, J., Clough, S. J., Ort, D. R., and DeLucia, E. H. 2010. Biotic stress globally downregulates photosynthesis genes. Plant Cell Environ. 33:1597-1613.

Brugger, A., Behmann, J., Paulus, S., Luigs, H.-G., Kuska, M. T., Schramowski, P., Kersting, K., Steiner, U., and Mahlein, A.-K. 2019b. Extending hyperspectral imaging for plant phenotyping to the UV-range. Remote Sens. 11:1401.

Brugger, A., Behmann, J., Paulus, S., Steiner, U., and Mahlein, A.-K. 2019a. Herausforderungen und Einschränkungen bei hyperspektralen Messungen im UV-Bereich. Workshop Computer-Bildanalyse in der Landwirtschaft. 25: 70-75.

Brugger, A., Schramowski, P., Paulus, S., Steiner, U., Kersting, K., and Mahlein, A.-K. 2021. Spectral signatures in the UV range can be combined with secondary plant metabolites by deep learning to characterize barley–powdery mildew interaction. Plant Pathol. 70:1572-1582.

Couture, J. J., Singh, A., Rubert-Nason, K. F., Serbin, S. P., Lindroth, R. L., and Townsend, P. A. 2016. Spectroscopic determination of ecologically relevant plant secondary metabolites. Methods Ecol. Evol. 7:1402-1412.

Csepregi, K., Kocsis, M., and Hideg, É. 2013. On the spectrophotometric determination of total phenolic and flavonoid contents. Acta Biol. Hung. 64:500-509.

Davoli, P., and Weber, R. W. 2002. Identification and quantification of carotenoid pigments in aeciospores of the daisy rust fungus, *Puccinia distincta*. Phytochemistry 60:309-313.

Fodor, J., Gullner, G., Adam, A. L., Barna, B., Komives, T., and Király, Z. 1997. Local and systemic responses of antioxidants to tobacco mosaic virus infection and to salicylic acid in tobacco (role in systemic acquired resistance). Plant Physiol. 114:1443-1451.

Galili, T. 2015. dendextend: An R package for visualizing, adjusting and comparing trees of hierarchical clustering. Bioinformatics 31: 3718-3720.

Gil, M. I., Ferreres, F., and Tomás-Barberán, F. A. 1998. Effect of modified atmosphere packaging on the flavonoids and vitamin c content of minimally processed Swiss chard (*Beta vulgaris* subspecies *cycla*). J. Agric. Food Chem. 46:2007-2012.

Hiscox, J., and Israelstam, G. 1979. A method for the extraction of chlorophyll from leaf tissue without maceration. Can. J. Bot. 57:1332-1334.

Jiang, J., Shao, Y., Li, A., Lu, C., Zhang, Y., and Wang, Y. 2013. Phenolic composition analysis and gene expression in developing seeds of yellow- and black-seeded *Brassica napus*. J. Integr. Plant Biol. 55:537-551.

Jing, L., Jinbao, J., Yunhao, C., Yuanyuan, W., Wei, S., and Wenjiang, H. 2007. Using hyperspectral indices to estimate foliar chlorophyll a concentrations of winter wheat under yellow rust stress. N.Z. J. Agric. Res. 50: 1031-1036.

Jones, J. D., and Dangl, J. L. 2006. The plant immune system. Nature 444: 323-329.

Joudi, Z., Davari, M., Jahanbakhsh, S., Ebadi, A., and Parmoon, G. 2018. Effect of Cercospora leaf spot on photosynthetic pigments and antioxidant enzymes activity of different sugar beet cultivars. J. Sugar Beet. 34:75-91.

Knogge, W. 1996. Fungal infection of plants. Plant Cell 8:1711.

Kowalski, R., and Wolski, T. 2003. TLC and HPLC analysis of the phenolic acids in *Silphium perfoliatum* L. leaves, inflorescences and rhizomes. JPC-J. Planar Chromat. 16:230-236.

Kristoffersen, R., Hansen, A. L., Munk, L., Cedergreen, N., and Jørgensen, L. N. 2018. Management of beet rust in accordance with IPM principles. Crop Prot. 111:6-16.

Król, A., Amarowicz, R., and Weidner, S. 2014. Changes in the composition of phenolic compounds and antioxidant properties of grapevine roots and leaves (*Vitis vinifera* L.) under continuous of long-term drought stress. Acta Physiol. Plant. 36:1491-1499.

Kuhn, M. 2012. Variable importance using the caret package. J. Stat. Softw. 6.

Kuhn, M. 2020. *caret*: Classification and regression training. https://cran.r-project.org/web/packages/caret/caret.pdf

Leucker, M., Wahabzada, M., Kersting, K., Peter, M., Beyer, W., Steiner, U., Mahlein, A.-K., and Oerke, E.-C. 2017. Hyperspectral imaging reveals the effect of sugar beet quantitative trait loci on Cercospora leaf spot resistance. Funct. Plant Biol.44:1-9.

Liaw, A., and Wiener, M. 2002. Classification and regression by randomForest. R News 2/3:18-22. https://cran.r-project.org/doc/Rnews/Rnews_2002-3.pdf

Lu, Y., Chen, Q., Bu, Y., Luo, R., Hao, S., Zhang, J., Tian, J., and Yao, Y. 2017. Flavonoid accumulation plays an important role in the rust resistance of *Malus* plant leaves. Front Plant Sci. 8:1286.

Mahatma, M., Bhatnagar, R., Mittal, G., and Mahatma, L. 2011. Phenol metabolism in downy mildew resistant and susceptible genotypes of pearl millet. Arch. Phytopathol. Plant Prot. 44:623-636.

Mahlein, A.-K., Rumpf, T., Welke, P., Dehne, H.-W., Plümer, L., Steiner, U., and Oerke, E.-C. 2013. Development of spectral indices for detecting and identifying plant diseases. Remote Sens. Environ. 128:21-30.

Mahlein, A.-K., Steiner, U., Dehne, H.-W., and Oerke, E.-C. 2010. Spectral signatures of sugar beet leaves for the detection and differentiation of diseases. Precis. Agric. 11:413-431.

Mahlein, A.-K., Steiner, U., Hillnhütter, C., Dehne, H.-W., and Oerke, E.-C. 2012. Hyperspectral imaging for small-scale analysis of symptoms caused by different sugar beet diseases. Plant Methods 8:1-13.

Meier, U., Bachmann, L., Buhtz, E., Hack, H., and Klose, R. 1993. Phänologische En- twicklungsstadien der Beta-Rüben (*Beta vulgaris* L. ssp.). Nachrichtenblatt des Deutschen Pflanzenschutzdienstes (Braunschweig) 45: 37-41.

Mihai, C. M., Mărghitaş, L. A., Bobiş, O., Dezmirean, D., and Tămaş, M. 2010. Estimation of flavonoid content in propolis by two different colorimetric methods. J. Anim. Sci. Biotechnol. 43:407-410.

Monici, M., Baglioni, P., Mulinacci, N., Baldi, A., and Vincieri, F. 1993. A research model on flavonoids as photoprotectors: Studies on the photochemistry of kaempferol and pelargonidin. International Symposium on Natural Phenols in Plant Resistance 381:340-347.

Morales, F., Cartelat, A., Álvarez-Fernández, A., Moya, I., and Cerovic, Z. G. 2005. Time-resolved spectral studies of blue-green fluorescence of artichoke (*Cynara cardunculus* L. var. *scolymus*) leaves: Identification of chlorogenic acid as one of the major fluorophores and age-mediated changes. J. Agric. Food Chem. 53:9668-9678.

Nabavi, S., Schmolze, D., Maitituoheti, M., Malladi, S., and Beck, A. H. 2016. Emdomics: A robust and powerful method for the identification of genes differentially expressed between heterogeneous classes. Bioinformatics 32:533-541.

Nagasubramanian, K., Jones, S., Singh, A. K., Sarkar, S., Singh, A., and Ganapathysubramanian, B. 2019. Plant disease identification using explainable 3D deep learning on hyperspectral images. Plant Methods 15:98.

Natella, F., Nardini, M., Di Felice, M., and Scaccini, C. 1999. Benzoic and cinnamic acid derivatives as antioxidants: Structure-activity relation. J. Agric. Food Chem. 47:1453-1459.

Paulus, S., and Mahlein, A.-K. 2020. Technical workflows for hyperspectral plant image assessment and processing on the greenhouse and laboratory scale. Gigascience 9:1-10.
Petkovšek, M. M., Stampar, F., and Veberic, R. 2008. Increased phenolic content in apple leaves infected with the apple scab pathogen. J. Plant Pathol. 90: 49-55.
Polder, G., Blok, P. M., de Villiers, H. A., van der Wolf, J. M., and Kamp, J. 2019. Potato virus Y detection in seed potatoes using deep learning on hyperspectral images. Front. Plant Sci. 10:209.
Pollock, C., and Drysdale, R. 1976. The role of phenolic compounds in the resistance of tomato cultivars to *Verticillium alboatrum*. J. Phytopathol. 86: 56-66.
Pusztahelyi, T., Holb, I. J., and Pócsi, I. 2015. Secondary metabolites in fungus−plant interactions. Front Plant Sci. 6:573.
Pyo, Y.-H., Lee, T.-C., Logendra, L., and Rosen, R. T. 2004. Antioxidant activity and phenolic compounds of Swiss chard (*Beta vulgaris* subspecies *cycla*) extracts. Food Chem. 85:19-26.
R Core Team, 2020: R: A Language and Environment for Statistical Computing. R Foundation for Statistical Computing, Vienna, Austria. https://www.R-project.org/
Ravn, H., Andary, C., Kovács, G., and Mølgaard, P. 1989. Caffeic acid esters as in vitro inhibitors of plant pathogenic bacteria and fungi. Biochem. Syst. Ecol. 17:175-184.
Ribeiro do Prado, L., Klock, S. A. L., Filho Wordell, J., A., Tramontin, M. A., Trapp, M. A., Mithöfer, A., and Nansen, C. 2018. Hyperspectral imaging to characterize plant–plant communication in response to insect herbivory. Plant Methods 14:1-11.
Santin, M., Neugart, S., Castagna, A., Barilari, M., Sarrocco, S., Vannacci, G., Schreiner, M., and Ranieri, A. 2018. UV-B pretreatment alters phenolics response to *Monilinia fructicola* infection in a structure-dependent way in peach skin. Front. Plant Sci. 9:1598.
Schmidt, S., Zietz, M., Schreiner, M., Rohn, S., Kroh, L. W., and Krumbein, A. 2010. Identification of complex, naturally occurring flavonoid glycosides in kale (*Brassica oleracea* var. *sabellica*) by high-performance liquid chromatography diode-array detection/electrospray ionization multi-stage mass spectrometry. Rapid Commun. Mass Spectrom. 24:2009-2022.
Scholes, J., Lee, P., Horton, P., and Lewis, D. 1994. Invertase: Understanding changes in the photosynthetic and carbohydrate metabolism of barley leaves infected with powdery mildew. New Phytol. 126:213-222.
Schramowski, P., Stammer, W., Teso, S., Brugger, A., Herbert, F., Shao, X., Luigs, H.-G., Mahlein, A.-K., and Kersting, K. 2020. Making deep neural networks right for the right scientific reasons by interacting with their explanations. Nat. Mach. Intell. 2:476-486.
Skadhauge, B., Thomsen, K. K., and Von Wettstein, D. 1997. The role of the barley testa layer and its flavonoid content in resistance to *Fusarium* infections. Hereditas 126:147-160.
Taniguchi, M., and Lindsey, J. S. 2018. Database of absorption and fluorescence spectra of >300 common compounds for use in photochem CAD. Photochem. Photobiol. 94:290-327.
Treutter, D. 2006. Significance of flavonoids in plant resistance: A review. Environ. Chem. Lett. 4:147.
Trocha, P., Daly, J., and Langenbach, R. 1974. Cell walls of germinating uredospores: I. Amino acid and carbohydrate constituents. Plant Physiol. 53:519-526.
Vergara-Diaz, O., Vatter, T., Kefauver, S. C., Obata, T., Fernie, A. R., and Araus, J. L. 2020. Assessing durum wheat ear and leaf metabolomes in the field through hyperspectral data. Plant J. 102:615-630.
Wang, Z., Chlus, A., Geygan, R., Ye, Z., Zheng, T., Singh, A., Couture, J. J., Cavender-Bares, J., Kruger, E. L., and Townsend, P. A. 2020. Foliar functional traits from imaging spectroscopy across biomes in eastern North America. New Phytol. 228:494-511.
Whetten, R., and Sederoff, R. 1995. Lignin biosynthesis. Plant Cell 7:1001.
Windels, C. E., Lamey, H. A., Hilde, D., Widner, J., and Knudsen, T. 1998. A Cerospora leaf spot model for sugar beet: In practice by an industry. Plant Dis. 82:716-726.
Yahya, M., Saeed, N. A., Nadeem, S., Hamed, M., and Saleem, K. 2020. Effect of leaf rust disease on photosynthetic rate, chlorophyll contents and grain yield of wheat. Arch. Phytopathol. Plant Prot. 53:425-439.